STUDY OF HYDROGEN BONDINGS IN PHENOL-AMINE ADDUCTS

MOHD MUSTAQIM BIN ROSLI

UNIVERSITI SAINS MALAYSIA

2008

STUDY OF HYDROGEN BONDINGS IN PHENOL-AMINE ADDUCTS

by

MOHD MUSTAQIM BIN ROSLI

Thesis submitted in fulfillment of the requirements
for the Degree of
Master of Science

May 2008

ACKNOWLEDGEMENTS

I would like to thank my parents, Rosli Bin Muhamed and Mahiran Binti Daud for their patience, encouragement and for always being very supportive.

My deep gratitude to Prof. Fun Hoong Kun, my principal supervisor and Prof. Lee Beck Sim, my co-supervisor for their guidance, useful advice and ideas throughout this project. My appreciation also goes to Dr. Abdul Razak Ibrahim, Dr. Suchada Chantrapromma and Dr. Ong Lye Hock.

I would like to express my appreciation to the Malaysian Government for the Scientific Advancement Grant Allocation (SAGA), account No. 304/PFIZIK/653003 and ScienceFund, account No. 304/PFIZIK/635028 for the post of research officer.

Thanks to the School of Physics and Institute of Graduate Studies, Universiti Sains Malaysia for giving me a chance to use all the facilities at this institution.

Finally, thank you to Mr. Khairul Arifin Mohd Noh, Mr. Azhar Abdul Rahman, Mr. Karunakaran, Mr. Mohamed Mustaqim Abu Bakar and everybody involved in this project directly or indirectly.

TABLE OF CONTENTS

Page

CHAPTER 3 – EQUIPMENT AND METHODOLOGY

CHAPTER 4 – RESULTS AND DISCUSSION

Page

LIST OF TABLES

LIST OF FIGURES

Page

LIST OF ABBREVIATIONS

CCD	Charged-Coupled Device
R	Reliability Index
SADABS	Siemens Area Detector Absorption Correction
SAINT	SAX Area-detector Integration (SAX – Siemens Analytical X-ray)
SMART	Siemens Molecular Analysis Research Tools
wR	Weight Reliability Index

KAJIAN IKATAN HIDROGEN DI DALAM SEBATIAN FENOL-AMINA

ABSTRAK

Lima sampel telah disediakan bagi tujuan mengkaji transisi fasa yang disebabkan oleh ikatan hidrogen di dalam sebatian fenol-amina. Sampel-sampel tersebut adalah (I) 2-Metilquinolinium 2,4-dinitrobenzoat, (II) 1:1 sebatian asid 3,5-dinitrobenzoik dan quinolin, (III) Hexametilenetetraminium 2,4-dinitrobenzoat monohidrat, (IV) 4-Aza-1-azoniabisiklo[2.2.2]oktan 2,4-dinitrobenzoat dan (V) Hexametilenetetraminium 3,5-dinitrobenzoat hemihidrat. Kaedah kristalografi sinar-X hablur tunggal telah digunakan untuk menentukan sama ada berlaku sebarang perubahan parameter kekisi pada suhu bilik dan 100K.

Beberapa ikatan hidrogen diperhatikan pada kesemua sampel. Walaubagaimanapun hanya sampel (V) yang menunjukkan fenomena transisi fasa dimana nilai parameter kekisi yang berbeza diperhatikan pada suhu bilik dan 100K (gandaan nilai paksi-*c*). Bagi sampel (V), kajian kebersandaran suhu dijalankan untuk mencari suhu kritikal T_c. Dari keputusan yang diperolehi, didapati ianya merupakan transisi fasa darjah pertama, dimana perubahan parameter kekisi berlaku secara tidak selanjar pada suhu T_c = 129K. Kes darjah pertama ini juga telah diterangkan secara makroskopik dengan menggunakan teori fenomenalogikal Landau.

Kaedah alternatif untuk mengira sifat-sifat termodinamik bagi suatu sistem transisi fasa darjah kedua yang disebabkan interaksi ikatan hidrogen dan fonon bagi hablur juga dilakukan di dalam kajian ini. Kajian tersebut dilakukan dengan memisahkan terus pembolehubah pseudo-spin dan hanya mengambil kira

pembolehubah pseudo-spin semasa mengira tenaga bebas. Keputusan yang diperolehi bersetuju dengan keputusan yang telah diterbitkan dahulu.

STUDY OF HYDROGEN BONDINGS IN PHENOL-AMINE ADDUCTS

ABSTRACT

Five samples have been prepared to study the phase transition caused by hydrogen bonds in phenol-amine adducts. Those samples are (I) 2-Methylquinolinium 2,4-dinitrobenzoate, (II) the 1:1 adduct of 3,5-dinitrobenzoic acid and quinoline, (III) Hexamethylenetetraminium 2,4-dinitrobenzoate monohydrate, (IV) 4-Aza-1-azoniabicyclo[2.2.2]octane 2,4-dinitrobenzoate and (V) Hexamethylenetetraminium 3,5-dinitrobenzoate hemihydrate. Single crystal X-ray crystallography method has been used to determine whether there are any changes in lattice parameters at room temperature and 100K.

A number of hydrogen bonds were observed in all the samples. However only sample (V) showed a phase transition phenomena in which different lattice parameter values were observed at room temperature and 100K (doubling the *c*-axis value). For sample (V), temperature dependence studies were done to find the critical temperature T_c. From the result, we know that this is a first order phase transition where the changes of the unit cell parameters occur discontinuously at the transition temperature T_c = 129K. This first order case is also explained macroscopically using Landau phenomenological theory.

An alternative method of calculating the thermodynamic properties of a system with the second-order phase transition caused by interaction of hydrogen bonds and phonon of the crystal was also done in this study. This was carried out by separating out the pseudo-spin variables completely and using only pseudo-spin

variables when calculating the free energy. The results agree with the previous published results.

CHAPTER 1

INTRODUCTION

1.1 Brief Description About Hydrogen Bonding

Hydrogen bonding plays an important role in molecular structure, including the biomolecules and it is still not fully understood. Its presence can affect the physical properties of gases, liquids and solids (Jeffrey, 1997). In supramolecular chemistry, the hydrogen bond is able to control and direct the structures of molecular assemblies because it is sufficiently strong and directional (Desiraju and Steiner, 1999). In mechanistic biology, it is believed to be responsible for the well-known base pairing in nucleic acids and for the secondary structure of proteins. It also influences the catalytic action of many enzymes and for the binding specificity of enzymes inhibitors (Perrin, 1994).

The hydrogen bond is said to exist if there is evidence of bond and the bond involves a hydrogen atom already bonded to another atom (Pimentel and McClellan, 1960). Hydrogen bonds are formed when the electronegative atom σ (σ = C, O, N, S, Cl *et al.,*) relative to H in σ-H covalent bond is such as to withdraw electrons and leave the proton unshielded. To interact with this donor σ-H bond, the acceptor κ must have lone-pair electrons or polarizable π-electrons. In general, a hydrogen bond can be characterized as a proton shared by two lone electron pairs. Hydrogen bond donor strengths are qualitatively proportional to these differences in electronegativity, F-H > O-H > N-H > C-H and the hydrogen bond has a directional property, being strongest when σ-H…κ =180°. The distance between the donor σ and acceptor κ atoms should be less than the sum of the Van der Waals radii of σ and κ (Jeffrey, 1997).

The typical hydrogen bond can be shown in scheme as follows,

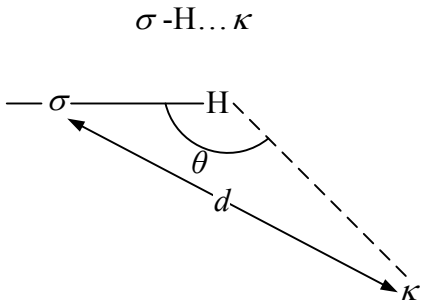

Figure 1.1 – Schematic of hydrogen bonds.

σ-H is the covalent bond length, H…κ is the hydrogen bond length and σ…κ is the hydrogen bond distance. These quantities define the σ-H…κ hydrogen bond angle, θ (Fig. 1.1).

Jeffery (1997) divides the hydrogen bonds into three categories (Table 1.1).

Table 1.1 – Properties of strong, moderate and weak hydrogen bonds.

	Strong	**Moderate**	**Weak**
σ-H…κ interaction	mostly covalent	mostly electrostatic	electrostatic
Bond lengths	σ-H ≈ H…κ	σ-H < H…κ	σ-H<<H…κ
H…κ (Å)	1.2 – 1.5	1.5 – 2.2	2.2 – 3.2
σ…κ (Å)	2.2 – 2.5	2.5 – 3.2	3.2 – 4.0
Bond Angles (°)	175 - 180	130 - 180	90 – 150
Bond energy (kcal mol^{-1})	14 - 40	4 – 15	< 4

Strong hydrogen bonds (ionic hydrogen bonds) are formed by groups in which there is a deficiency of electron density in the donor group ($-\overset{+}{O}-H$, $\equiv\overset{+}{N}-H$) or an excess of electron density in the acceptor group ($\overset{-}{F}$, $\overset{-}{O}-H$, $\overset{-}{O}-C$). Moderate hydrogen bonds are formed by neutral donor and acceptor groups

($-O-H$, $-N(H)-H$), in which the donor A atoms are electronegative relative to hydrogen and the acceptor B atoms have lone-pair unshared electrons. Weak hydrogen bonds are formed when the hydrogen atom is covalently bonded to a more electro-neutral atom relative to hydrogen ($C-H$, $Si-H$) or the acceptor group has no lone-pairs but has π electrons, such as $C \equiv C$ or an aromatic ring (Jeffrey, 1997).

1.2 Hydrogen Bonding, Phenol-Amine Adducts and Phase Transitions

Phenol-amine adducts in solid state form are widely used to study hydrogen bonds (Coupar, Glidewell and Ferguson, 1997; Sobcyzk *et al.,* 2000; Chantrapromma, 2004) especially hexamethylenetetramine crystals. This is because phenol or organic acids and amine bases in solid phase generally interacted by intramolecular or intermolecular O-H…O, O-H…N or N-H…O hydrogen bonds (Desiraju, 1995; Chantrapromma *et al.,* 2006). From all these previous studies (Coupar, Glidewell and Ferguson, 1997; Sobcyzk *et al.,* 2000; Chantrapromma, 2004), normally in hexamethylenetetramine crystals, there are more than two hydrogen bonds that can be observed.

Chantrapromma in her thesis (2004) studied the different categories of hydrogen bondings formed by adducts possessing different relative strengths of acidity (pK_a) and basicity (pK_b) of the starting materials and also the role of steric effect of the components of the adducts. In the study, she and the group found a new second order temperature-dependent reversible ferroelastic phase transition which was named as FAST (Fun-Anwar-Suchada Transition) occurring in three samples [hexamethylenetetraminium 2,4-dinitrophenolate monohydrate (HMTDNP), hexamethylenetetraminium 3,5-dinitrobenzoate-3,5-dinitrobenzoic acid monohydrate (HMT2DNBW) and quinuclidinium 2,4-dinitrophenolate (QNCDNP)]. There are

two types of transition; orthorhombic-to-monoclinic and monoclinic-to-triclinic were observed. This newly found phase transition has been explained macroscopically using the Landau phenomenological theory (Fun *et al.,* 2003) and also microscopically using the pseudo-spin approach (How *et al.,* 2005).

The microscopic theory of this new type of phase transition is based on the idea that the main mechanism responsible for phase transition is interaction of hydrogen bonds with the lattice vibrations or phonons of the crystal. The hydrogen bonds are modelled as two-level systems, and described by pseudo-spin variables. The starting Hamiltonian used in the model is a combination of harmonic phonon Hamiltonian H_p, and the interaction energy of the additional hydrogen bonds H_s (How *et al.,* 2005).

Studies on hydrogen bonding in phenol-amine adducts can be used as a model for the more complicated hydrogen bonding in biological systems (Blow, 1976; Chantrapromma, 2004). It is worthwhile to understand the phase transitions caused by hydrogen bonds since hydrogen bonds occur in a large class of materials.

1.3 X-ray Crystallography

X-ray crystallography is a powerful method which enables researchers to obtain a detailed picture of the contents of the crystal at the atomic level. By using this method, researcher can calculate interatomic distances and bond lengths to get a complete three dimensional picture of the molecules inside the crystals. Other features such as planarity of a particular group of the atoms, the angles between planes and the torsion angles around bonds can also be calculated.

However, to use this method, the samples must be in single crystal form. An ideal crystal is constructed by an infinite repetition of identical structural units in

space. The structure of all crystals can be described in terms of lattice, with a group of atoms attached to every lattice point. The lattice is defined by three fundamental translation vectors **a**, **b** and **c**. These vectors may also be described in terms of their lengths (a, b, c) and the angles between them (α, β, γ) (Fig. 1.2). These lengths and angles are the lattice constants or lattice parameters of the unit cell. The volume of a parallelepiped with axes a, b and c is

$$V_C = |a \times b \times c|$$

by elementary vector analysis (Kittel, 1996).

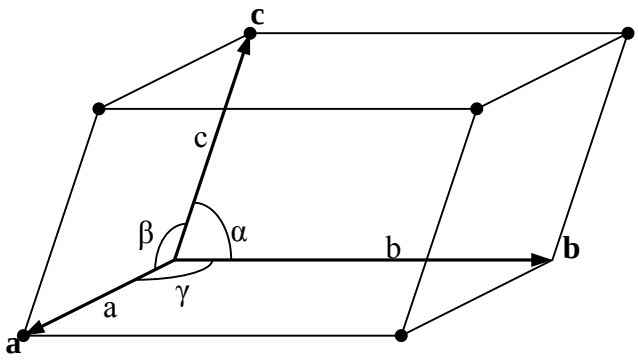

Figure 1.2 – Crystal lattice

X-rays lie in the electromagnetic spectrum between ultraviolet and gamma radiation in which the approximate range of wavelengths is 0.1 – 100 Å, depending on the energy of the electron that produced the X-ray. X-ray is generated when electrons are accelerated by an electric field and directed against a metal target, which slows them rapidly by multiple collisions (Stout and Jensen, 1989). This produces the continuous spectrum. The characteristic spectrum is produced when the

electron in the innermost shells of the atoms are dislodged by the bombarding electrons.

The basic parts of an X-ray tube are source of electrons (cathode electrode) and metal target (anode electrode) that emit the X-ray. Nowadays, the most common used X-ray tube is hot cathode tube which was invented by W. D. Coolidge in 1913 (Figure 1.3). Electrons are liberated from heated filament and accelerated by a high voltage towards the metal target. Because of the high voltage through which the electrons are accelerated, the power dissipated at the anode is quite large. In order to prevent the anode from melting, the X-ray tube is equipped with a cooling system. Additional cooling can be achieved by using a rotary anode. The rotating anode can handle much higher energy delivered by the electrons and data collections can be taken at shorter times compared to those with stationary anodes (Cullity, 1956; Stout and Jensen, 1989).

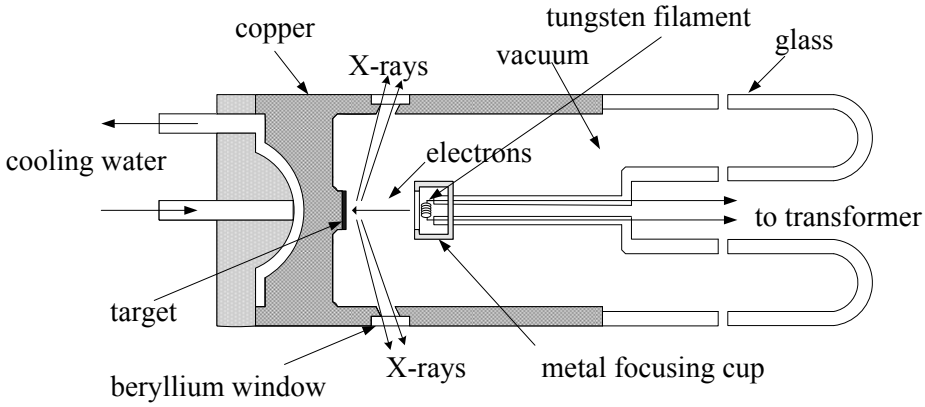

Figure 1.3 – Cross section of sealed-off filament X-ray tube (schematic) (Cullity, 1956).

The details of how this method works shall be explained in chapter 2 and chapter 3.

1.4 Landau Theory

Landau theory is a thermodynamic theory that can be used to explain the behaviors of the crystal at phase transition. It is based on a power series expansion of the free energy of the crystal with respect to an order parameter of the crystal. By using the landau theory, the thermodynamics of the crystal such as free energy or heat capacity can be directly linked to crystal lattice parameters and the relation between these quantities (crystal thermodynamics and crystal lattice parameters) can show how they can be changed by the influence of temperature or pressure (Stanley, 1971).

1.5 Objectives

In these studies, X-ray crystallography was used to get a clear picture of the molecules, crystal packing and hydrogen bonds in the crystal of some phenol-amine adducts. This method was also being used to find whether there was any phase transition in the samples studied by looking at the crystal systems and the lattice parameters as a function of temperature. The main objective of this study was to find more examples of phenol-amine adducts that exhibit the Fun-Anwar-Suchada Transition (FAST) phenomena.

Another objective of this study was to verify the previous calculation of the microscopic theory that explains the second order FAST phenomena (How *et al.,* 2005). For this calculation, we attempted to derive an effective Hamiltonian which contains only pseudo-spin variables.

This study was to obtain more details on the fundamental knowledge of the FAST phase transition in phenol-amine adducts which is caused by the interaction of hydrogen bonds and the phonons of the crystals.

CHAPTER 2

PRINCIPLES OF X-RAY CRYSTALLOGRAPHY

2.1 X-ray Diffraction

Diffraction can be described as a combination of scattering and interference phenomenon (Ladd and Palmer, 1993). Referring to the figure 2.1, consider an X-ray beam incident on a pair of parallel plane of A and B separated by the distance *d*. The parallel incident rays 1 and 2 make an angle θ with the A and B planes. Due to interference effects, only the parallel reflections ray 1' and 2' at angle θ will result (if the waves represented by these rays are in phase).

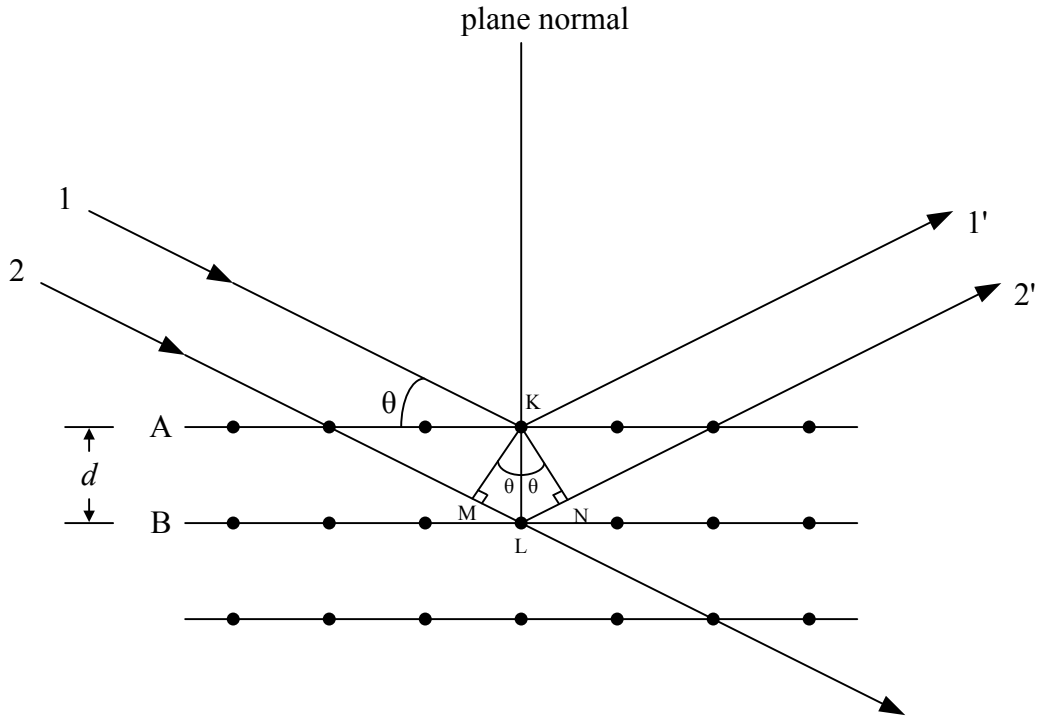

Figure 2.1 – Diffraction of X-ray by a crystal (Cullity, 1956).

From figure 2.1, it is obvious that $\angle MKL = \angle NKL = \theta$ and ML = NL. With this we can derive that,

$$ML + NL = 2ML \tag{2.1}$$

and this equals with the integral number of wavelengths λ for constructive interference.

$$2ML = n\lambda \tag{2.2}$$

By using trigonometry law

$$ML / d = \sin\theta$$

we get

$$2d \sin\theta = n\lambda \quad \rightarrow \textit{Bragg's Law} \tag{2.3}$$

2.2 Argand Diagram

An Argand diagram can be used to represent clearly the combination of waves. In an Argand diagram, waves are represented as vectors with real and imaginary component.

$$\boldsymbol{f_1} = f_1 \cos\varphi_1 + \mathrm{i} f_1 \sin\varphi_1 \tag{2.4}$$

$$\boldsymbol{f_2} = f_2 \cos\varphi_2 + \mathrm{i} f_2 \sin\varphi_2 \tag{2.5}$$

$$\boldsymbol{F} = \boldsymbol{f_1} + \boldsymbol{f_2}$$

These equations are illustrated in figure 2.2.

De Moivre's theorem states that

$$\mathbf{e}^{\pm \mathrm{i}\varphi} = \cos\varphi + \mathrm{i}\sin\varphi \tag{2.6}$$

Using this theorem, equation 2.4 and 2.5 becomes

$$\boldsymbol{f_1} = f_1 \mathbf{e}^{\mathrm{i}\varphi_1} \quad , \quad \boldsymbol{f_2} = f_2 \mathbf{e}^{\mathrm{i}\varphi_2} \tag{2.7}$$

$$\therefore \quad \boldsymbol{F} = f_1 \mathbf{e}^{\mathrm{i}\varphi_1} + f_2 \mathbf{e}^{\mathrm{i}\varphi_2} \tag{2.8}$$

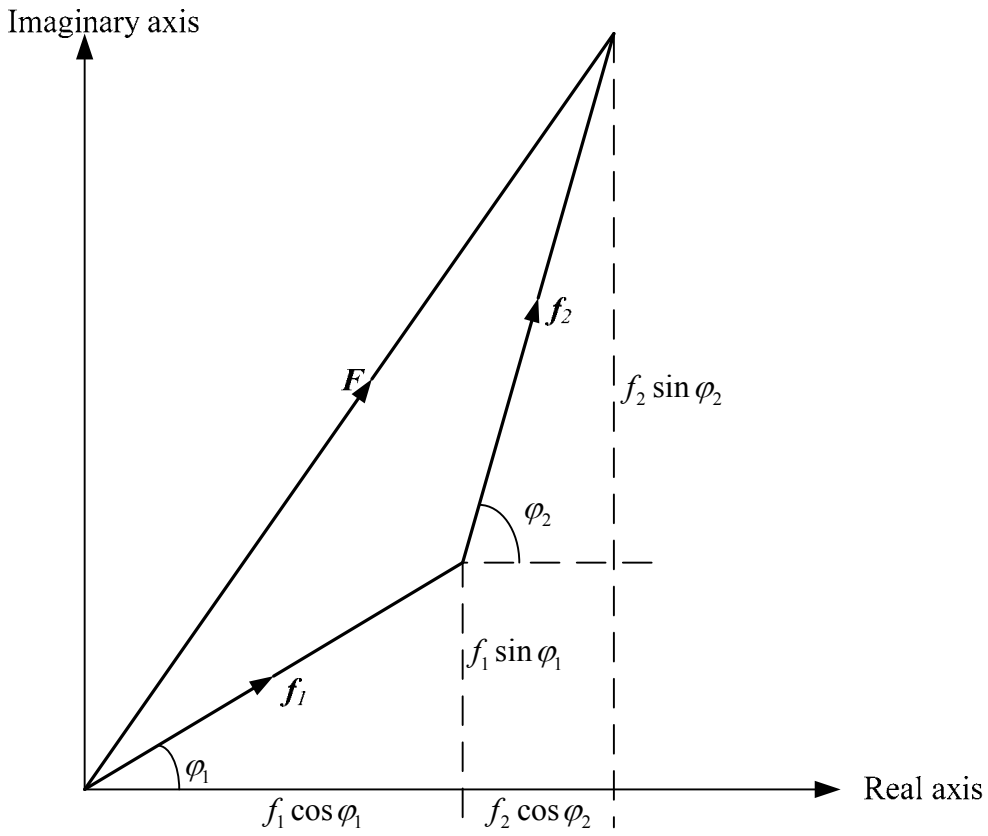

Figure 2.2 – Combination of two waves, f_1 and f_2 on an Argand diagram (Ladd and Palmer, 1993).

2.3 Combination of *N* Waves

Using the same methods, we can combine any number of waves. The resultant of *N* waves is,

$$\boldsymbol{F} = f_1\mathbf{e}^{\mathrm{i}\varphi_1} + f_2\mathbf{e}^{\mathrm{i}\varphi_2} + \cdots + f_j\mathbf{e}^{\mathrm{i}\varphi_j} + \cdots + f_N\mathbf{e}^{\mathrm{i}\varphi_N} \tag{2.9}$$

or

$$\boldsymbol{F} = \sum_{j=1}^{N} f_j\mathbf{e}^{\mathrm{i}\varphi_j} \tag{2.10}$$

we can also express this equation using an Argand diagram

(Figure 2.3, for $N = 6$).

The resultant $\boldsymbol{F}$ is given by

$$\boldsymbol{F} = |F|\,\mathbf{e}^{i\varphi} \tag{2.11}$$

with $|F|^2 = \boldsymbol{F}\boldsymbol{F}^*$ and $\boldsymbol{F}^* = |F|\,\mathbf{e}^{-i\varphi}$

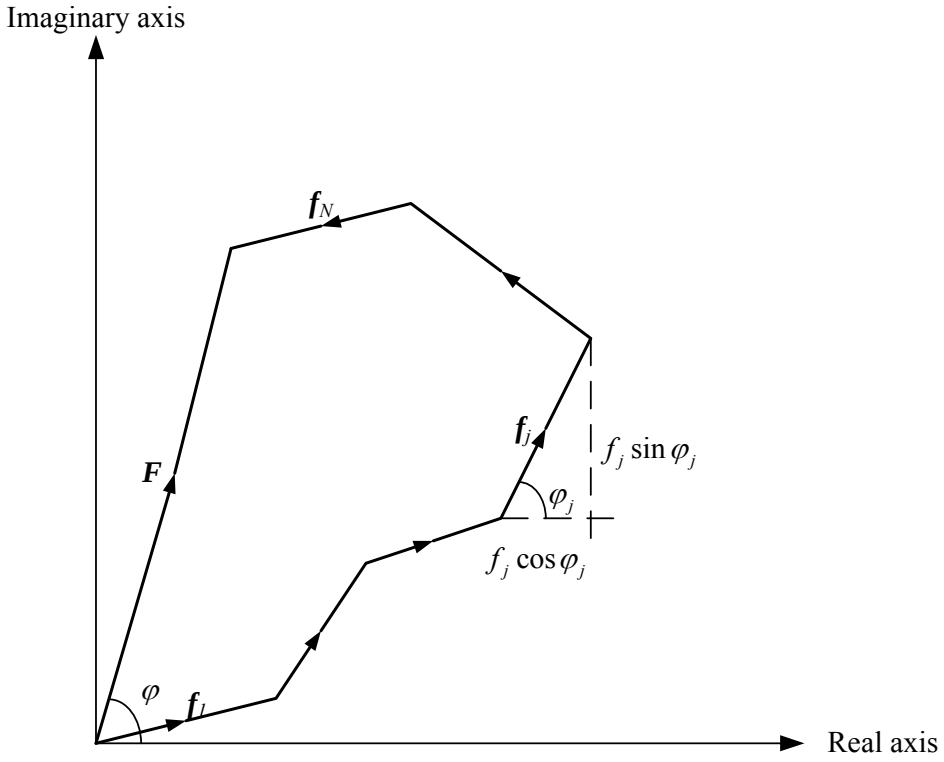

Figure 2.3 – Combination of N waves (N=6), $\boldsymbol{F} = \sum_{j=1}^{6} f_j \mathbf{e}^{i\varphi_j}$ using an Argand diagram (Ladd and Palmer, 1993).

2.4 Phase Difference

The phase difference associated with waves scattered by an atom j whose position relative to the origin is specified by the fractional coordinate's x_j, y_j, z_j is

$$\delta_j = \lambda(hx_j + ky_j + lz_j) \tag{2.12}$$

The corresponding phase difference in angular measure is

$$\varphi_j = (2\pi / \lambda)\delta_j \tag{2.13}$$

or

$$\varphi_j = 2\pi(hx_j + ky_j + lz_j) \tag{2.14}$$

2.5 Atomic Scattering Factor

Atomic scattering factor is the amplitude of the waves scattered by the atom and denoted as $f_{j,\theta}$. Atomic scattering factors are used to evaluate the combined scattering from all atoms in the unit cell. Its value depends on the nature of the atom, the wavelength of X-ray used and the thermal vibration of the atom (Ladd and Palmer, 1993).

The number of extra-nuclear electron in the atom can influence the value of $f_{j,\theta}$ (maximum value for given atom *j* is Z_j, the atomic number of the *j*th atomic species). Along the direction of the incident beam [$\sin\theta(hkl) = 0$], $f_{j,\theta}$ has its maximum value,

$$f_{j,\theta(\theta=0)} = Z_j \tag{2.15}$$

$f_{j,\theta}$ is expressed in number of electrons.

The atomic scattering factor is also influenced by the thermal vibration of a particular atom in a given crystal. Each atom in a structure vibrates anisotropically and the exact description of this motion involved several parameters which are dependent upon direction (Ladd and Palmer, 1993). In isotropic vibration (simpler case) the temperature factor correction for the *j*th atom is

$$T_{j,\theta} = \exp[-B_j(\sin^2\theta) / \lambda^2] \tag{2.16}$$

where

$$B_j = 8\pi 2\overline{U_j^2} \quad \rightarrow \text{temperature factor of atom } j \tag{2.17}$$

$\overline{U_j^2}$ is the mean-square amplitude of vibration of the *j*th atom from its equilibrium position in a direction normal to the reflecting plane, and is a function of temperature. $T_{j,\theta}$ is a function of $(\sin\theta)/\lambda$ and *hkl*. The temperature-corrected atomic scattering factor may be written as:-

$$g_j = f_{j,\theta} T_{j,\theta} \tag{2.18}$$

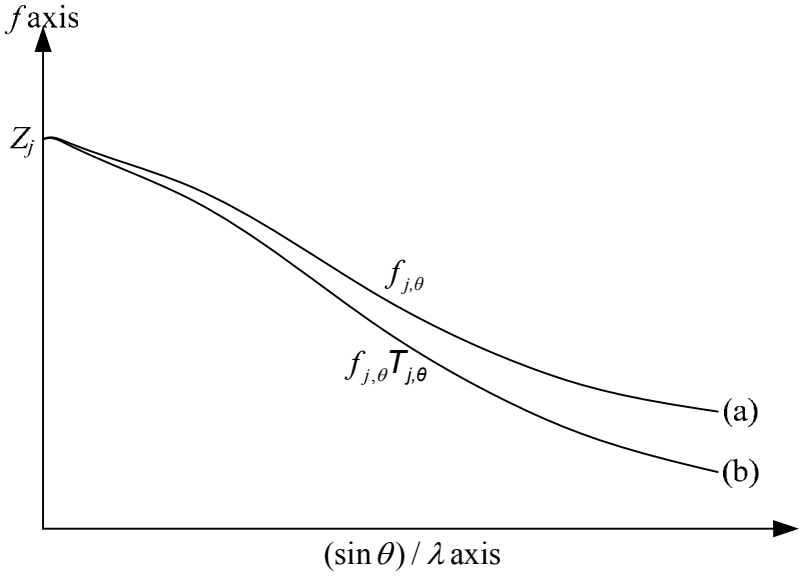

Figure 2.4 – Atomic scattering factors: a) stationary atom, $f_{j,\theta}$, b) atom corrected for thermal vibration $f_{j,\theta}T_{j,\theta}$ (Ladd and Palmer, 1993).

2.6 Structure Factor

The structure factor ***F(hkl)*** express the combined scattering of X-rays for all atoms in the unit cell compared to a single electron and its amplitude |*F(hkl)*| is measured in electrons. The value is expressed in term of $g_j (g_{j,\theta} \equiv g_j)$ and $\varphi_j [\varphi_j(hkl) \equiv \varphi_j]$ (Ladd and Palmer, 1993). From equation 2.9, the resultant wave for the unit cell is therefore

$$\left.\begin{aligned} \boldsymbol{F}(hkl) &= \sum_{j=1}^{N} g_j \mathbf{e}^{\mathrm{i}\varphi_j} \\ &= \sum_{j=1}^{N} g_j \exp[\mathrm{i}2\pi(hx_j + ky_j + lz_j)] \end{aligned}\right\} \tag{2.19}$$

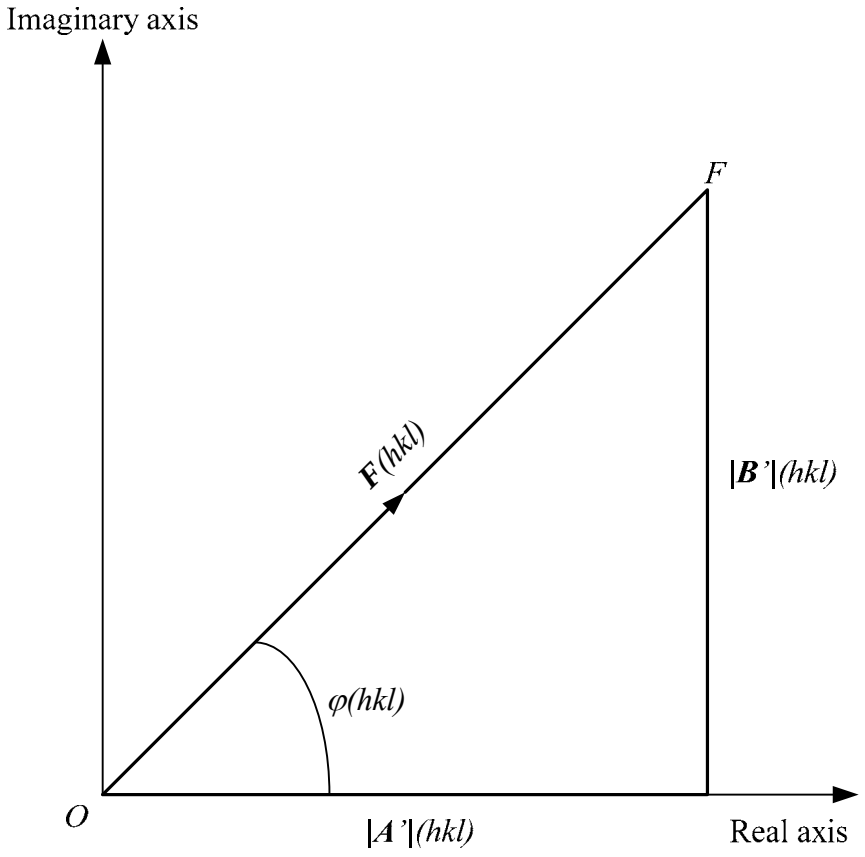

Figure 2.5 – Structure factor ***F****(hkl)* plotted on Argand diagram; $\varphi(hkl)$ is the resultant phase, and the amplitude $|\boldsymbol{F}(hkl)|$ is represented by length of *OF* (Ladd and Palmer, 1993).

From figure 2.5

$$\boldsymbol{F}(hkl) = A'(hkl) + \boldsymbol{i}B'(hkl) \tag{2.20}$$

where $A' = |\boldsymbol{A}'|$ and $B' = |\boldsymbol{B}'|$.

$$A'(hkl) = \sum_{j=1}^{N} g_j \cos 2\pi(hx_j + ky_j + lz_j) \tag{2.21}$$

and

$$B'(hkl) = \sum_{j=1}^{N} g_j \sin 2\pi(hx_j + ky_j + lz_j) \tag{2.22}$$

$$\therefore \quad \boldsymbol{F}(hkl) = |F(hkl)|\,\mathbf{e}^{i\varphi(hkl)} \tag{2.23}$$

where the amplitude is given by

$$|F(hkl)| = [A'^2(hkl) + B'^2(hkl)]^{1/2} \tag{2.24}$$

and the phase by

$$\tan\varphi(hkl) = \frac{B'(hkl)}{A'(hkl)} \tag{2.25}$$

From figure 2.5 it may be seen that

$$A'(hkl) = |F(hkl)|\cos\varphi(hkl) \tag{2.26}$$

and

$$B'(hkl) = |F(hkl)\sin\varphi(hkl) \tag{2.27}$$

2.7 Friedel's Law

A diffraction pattern may be thought of as a reciprocal lattice with each point weighted by corresponding value of $|F(hkl)|$ or $I(hkl)$.

Therefore $I(hkl) \propto |F(hkl)|^2$ (2.28)

Friedel's law states the centrosymmetric property of the diffraction pattern as

$$I(hkl) = I(\bar{h}\bar{k}\bar{l}) \tag{2.29}$$

The g_j value is same for the *hkl* and $\bar{h}\bar{k}\bar{l}$ reflection since atomic scattering factor is a factor of $[(\sin\theta)\lambda]^2$.

i.e. $g_{j,\theta} = g_{j,-\theta}$ (2.30)

because reflection from opposite sides of any planes will occur at the same Bragg angle, θ. The dependence on the spherically symmetric model of an atom, which is generally assumed in the calculation of f values, should be noted. From 2.19

$$\boldsymbol{F}(hkl) = \sum_{j=1}^{N} g_{j,\theta} \exp[\mathrm{i}2\pi(hx_j + ky_j + lz_j)] \tag{2.31}$$

and

$$\boldsymbol{F}(\bar{h}\bar{k}\bar{l}) = \sum_{j=1}^{N} g_{j,-\theta} \exp[-\mathrm{i}2\pi(hx_j + ky_j + lz_j)] \tag{2.32}$$

From 2.20

$$\boldsymbol{F}(\bar{h}\bar{k}\bar{l}) = A'(\bar{h}\bar{k}\bar{l}) + \mathbf{i}B'(\bar{h}\bar{k}\bar{l}) \tag{2.33}$$

where $A'(\bar{h}\bar{k}\bar{l})$ and $B'(\bar{h}\bar{k}\bar{l})$ are given by 2.21 and 2.22, respectively. From 2.21 and 2.22 we get

$$\boldsymbol{F}(\bar{h}\bar{k}\bar{l}) = A'(hkl) - \mathbf{i}B'(hkl) \tag{2.34}$$

The vectorial representation of $\boldsymbol{F}(hkl)$ and $\boldsymbol{F}(\bar{h}\bar{k}\bar{l})$ are shown on Argand diagram on figure 2.6. From the figure,

$$\varphi(\bar{h}\bar{k}\bar{l}) = -\varphi(hkl) \tag{2.35}$$

$$|F(hkl)| = |F(\bar{h}\bar{k}\bar{l})| = [A'^2(hkl) + B'^2(hkl)]^{1/2} \tag{2.36}$$

From 2.28,

$$\mathrm{I}(hkl) = \mathrm{I}(\bar{h}\bar{k}\bar{l}) \quad \rightarrow \quad \textit{Friedel's Law} \tag{2.37}$$

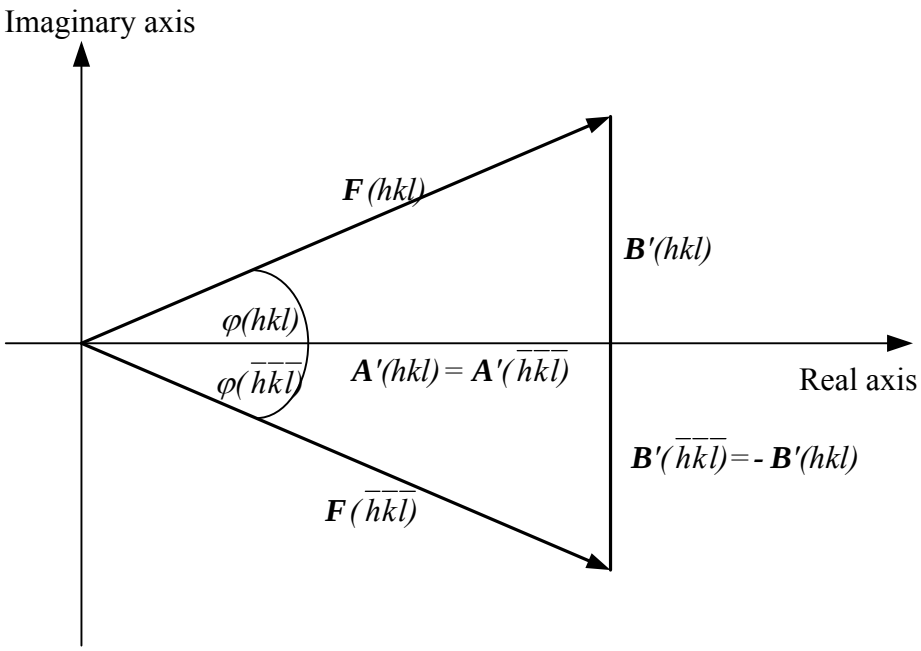

Figure 2.6 – Relationship between ***F(hkl)*** and ***F*** $(\bar{h}\bar{k}\bar{l})$ leading to Friedel's law(Ladd and Palmer, 1993).

2.8 Electron Density Distribution

X-ray are scattered by the electrons associated with the atoms in the crystal. Atom with high atomic numbers will give a greater concentration of electrons compared to atom with low atomic numbers. This concentration of electrons and its distribution around the atom is called the electron density ρ (measured in electrons per $Å^3$) (Ladd and Palmer, 1993).

The general electron density function is expressed as a three-dimensional Fourier series

$$\rho(x,y,z) = \frac{1}{V_c}\sum_{h}\sum_{\substack{k\\-\infty}}^{\infty}\sum_{l} \boldsymbol{F}(hkl)\exp[-\mathrm{i}2\pi(hx+ky+lz)] \tag{2.38}$$

By using 2.23, 2.38 becomes

$$\rho(x,y,z) = \frac{1}{V_c}\sum_{h}\sum_{\substack{k\\-\infty}}^{\infty}\sum_{l} |\boldsymbol{F}(hkl)|\,\mathbf{e}^{\mathrm{i}\varphi(hkl)}\mathbf{e}^{-\mathrm{i}2\pi(hx+ky+lz)} \tag{2.39}$$

This equation implies that the electron density is a complex function, but it is real throughout the unit cell, using 2.6, 2.20 and 2.34

$$\rho(x,y,z) = \frac{1}{V_c}\sum_h \sum_{k=-\infty}^{\infty} \sum_l \{A'(hkl)\cos[2\pi(hx+ky+lz)] + B'(hkl)\sin[2\pi(hx+ky+lz)]\} \tag{2.40}$$

- summations are taken over the appropriate practical value of *h*, *k*, and *l*.

Using 2.26 and 2.27, 2.40 becomes

$$\rho(x,y,z) = \frac{1}{V_c}\sum_h \sum_{k=-\infty}^{\infty} \sum_l |\boldsymbol{F}(hkl)| \cos[2\pi(hx+ky+lz) - \varphi(hkl)] \tag{2.41}$$

The process of X-ray diffraction corresponds to Fourier analysis or breakdown of the object $\rho(x,y,z)$ into its constituent term. However from experimental work, only intensities $I(hkl)$ can be measured meaning only the magnitude of $|\boldsymbol{F}(hkl)|$ is known since ($I(hkl) \propto |\boldsymbol{F}(hkl)|^2$) but not the phase. Fourier synthesis is equivalent to a summation of $\boldsymbol{F}(hkl)$ in order to reconstruct the object, but it cannot be achieved without regaining the phase information. The methods of structure analysis seek to extract phase information starting from $|\boldsymbol{F}_{o=observed}|$ data.

Electron density is concentrated in the vicinity of the atoms. Atom appears as peaks in the electron density function and the peak position of a given atom is assumed to correspond to its atomic center. Generally, the more complete and accurate the experimental $|\boldsymbol{F}|$ data, the better will be the atomic resolution and more precise the final structure model.

The heights of the peaks in an electron density distribution of a crystal are proportional to the corresponding atomic number. The hydrogen atom which has the lowest atomic number cannot be observed in electron density map because its small electron density merges into the background density (Ladd and Palmer, 1993).

2.9 Heavy Atom Method

2.9.1 Patterson Function

In 1934, Patterson discover a Fourier series using value of $|\mathbf{F}(hkl)|^2$ (which can be calculated directly from the experiment intensity data) as coefficient instead of *F(hkl)*. However, the result cannot be interpreted as a set of atomic positions (because no phase information was included in this series), but as a collection of interatomic vectors all taken to a common origin (Ladd and Palmer, 1993).

2.9.2 One-dimensional Patterson Function

The electron density at any fractional coordinates x and $x + u$ is $\rho(x)$ and $\rho(x+u)$ respectively. The average product of these two electron densities in a repeat length of a, for a given value of u is,

$$A(u) = \int_0^1 \rho(x)\rho(x+u)dx \tag{2.42}$$

Using 2.38 (in appropriate 1-D form)

$$A(u) = \int_0^1 \frac{1}{a^2} \sum_h \boldsymbol{F}(h)\mathbf{e}^{-i2\pi hx} \sum_{h'} \boldsymbol{F}(h')\mathbf{e}^{-i2\pi h'(x+u)}dx \tag{2.43}$$

- index *h'* lies within the same range as *h*.

Equation 2.43 can be write as

$$A(u) = \frac{1}{a^2} \sum_h \sum_{h'} \boldsymbol{F}(h)\boldsymbol{F}(h')\mathbf{e}^{-i2\pi h'u} \int_0^1 \mathbf{e}^{-i2\pi(h+h')x}dx \tag{2.44}$$

The integral $$\int_0^1 \mathbf{e}^{-i2\pi(h+h')x}dx = \frac{\mathbf{e}^{-i2\pi(h+h')x}}{-i2\pi(h+h')}\Bigg|_0^1 \tag{2.45}$$

$\mathbf{e}^{-i2\pi(h+h')}$ is unity, since h and h' are integers and the integral in general is zero. However, for value $h' = -h$, the integral becomes indeterminate.

$\rightarrow$ by substituting $h' = -h$ before integration,

$$\int_0^1 dx = 1$$

From 2.44, for nonzero values of $A(u)$, when $h' = -h$,

$$A(u) = \frac{1}{a^2} \sum_{h} \sum_{-h} \boldsymbol{F}(h)\boldsymbol{F}(-h)\mathbf{e}^{i2\pi hu} \tag{2.46}$$

Applying the Friedel's Law

$$\boldsymbol{F}(-h) = \boldsymbol{F}^*(h)$$

$$A(u) = \frac{1}{a^2} \sum_{h=-\infty}^{\infty} |\boldsymbol{F}(h)|^2 \, \mathbf{e}^{i2\pi hu} \tag{2.47}$$

$$A(u) = \frac{1}{a^2} \sum_{h=0}^{\infty} (|\boldsymbol{F}(h)|^2 \, \mathbf{e}^{i2\pi hu} + |\boldsymbol{F}(h)|^2 \, \mathbf{e}^{-i2\pi hu}) \tag{2.48}$$

From De-Moivre theorem

$$A(u) = \frac{2}{a^2} \sum_{h=0}^{\infty} (|\boldsymbol{F}(h)|^2 \cos 2\pi hu) \tag{2.49}$$

$\therefore$ the corresponding Patterson function $P(u)$ is usually defined as

$$P(u) = \frac{2}{a^2} \sum_{h=0}^{\infty} (|\boldsymbol{F}(h)|^2 \cos 2\pi hu) \tag{2.50}$$

2.9.3 Three-dimensional Patterson Function

For three-dimensional Patterson function we replace $\rho(x)$ and $\rho(x + u)$ with $\rho(x, y, z)$ and $\rho(x + u, y + v, z + w)$ respectively and integrate over a unit fractional volume.

Three-dimensional Patterson Function

$$P(u,v,w) = \frac{2}{V_c} \sum_{h} \sum_{k} \sum_{l} [|\boldsymbol{F}(hkl)|^2 \cos 2\pi(hu + kv + lw)] \tag{2.51}$$

- the summation range, with most general case over a one half of experimental reciprocal space.

By comparison with 2.41 and 2.51, this is a Fourier series with zero phases and $|F(hkl)|^2$ as coefficients. Since $|F(hkl)|^2$ is $\boldsymbol{F \cdot F^*}$ from 2.38, 2.51 represent the convolution of the electron density $\rho(\boldsymbol{r})$ with its inversion in the origin $\rho(\boldsymbol{r})$. In practice, 2.51 may be handled like the corresponding electron density equation with *u, v* and *w* replacing *x, y* and *z* but both functions explore the same thing, the unit cell.

2.9.4 Positions and Weights of Peaks in the Patterson Function

The positions of the peak in the Patterson function P(u, v, w) can be plotted in three-dimension by placing each atom of the unit cell of a structure in turn at the origin of Patterson space, in parallel orientation and mapping the positions of all other atoms on the Patterson unit cell. By doing this, we can see that all atoms and their translation equivalents produce vector peaks lying on the points of a lattice that is identical in shape and size to the crystal lattice.

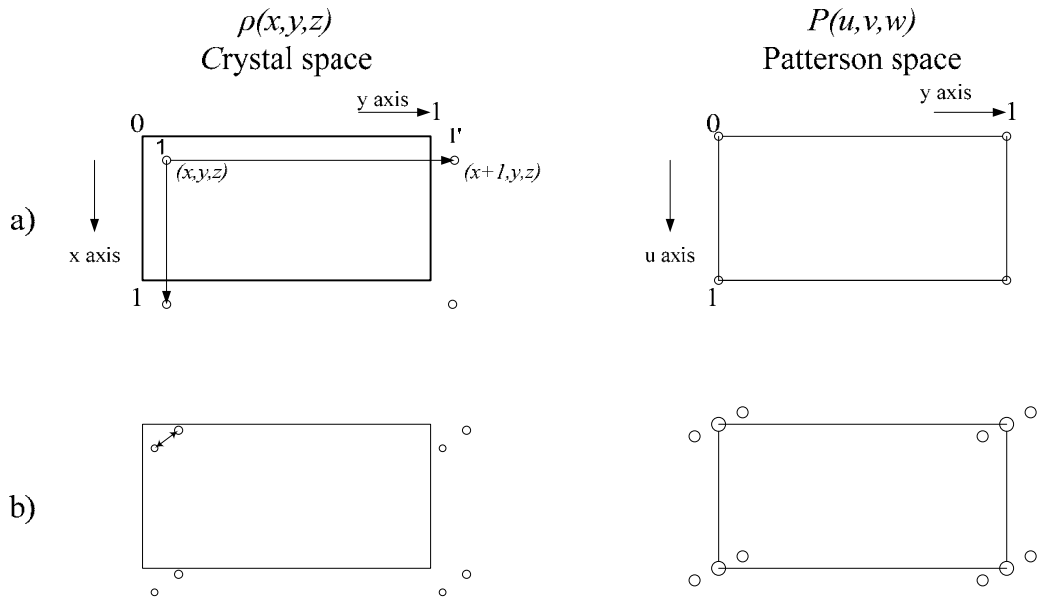

Figure 2.7 – Effects of symmetry-related and symmetry-independent atoms on the Patterson function (Ladd and Palmer, 1993).

Atom 1 at *x, y, z* and its translation equivalent at *1'*, at *x, 1+y, z* give rise to a vector ending at 0, 1, 0 in the Patterson map [see Figure 2.7(a)]. The height of the origin peak is given by,

$$P(0,0,0) = \frac{2}{V_c} \sum_{h=0} \sum_{k}^{\infty} \sum_{l=0} | \boldsymbol{F}_0(hkl) |^2 \tag{2.52}$$

Generally, 2.52 is equivalent to a superposition at the origin of all N products like $\rho(x_j,y_j,z_j)\ \rho(x_j,y_j,z_j)$, where N is the number of atoms in the unit cell. Since $\rho(x_j,y_j,z_j)$ is proportional to the atomic number Z_j of the jth atom,

$$P(0,0,0)\ \mu \sum_{j=1}^{N} Z_j^2 \tag{2.53}$$

A single vector interaction between two atoms j and k (Figure 2.7b) will have Patterson peak of height proportional to Z_jZ_k, Hence, the height $H(j,k)$ of this peak will be given by

$$H(j,k) \approx P(0,0,0) Z_j Z_k \ / \sum_{j=1}^{N} Z_j^2 \tag{2.54}$$

where P(0,0,0) is calculated from 2.52.

In a structure with N atoms per unit cell, each atom forms a vector with the remaining N-1 atoms. Thus we will have $N(N\text{-}1)$ nonorigin peaks and N superposed origin peaks. The Patterson unit cell is the same size and shape as the crystal unit cell, but it has accommodate N^2 rather than N peaks and is therefore correspondingly overcrowded. Therefore, peaks in Patterson space tend to overlap when there are many atoms in the unit cell (Ladd and Palmer, 1993).

2.9.5 Sharpened Patterson Function

To reduce overlapping, the sharpened Patterson function is used. In a conceptual point atom, the electrons would be concentrated at a point. The atomic scattering factor curves (Figure 2.4) would be parallel to the abscissa and f would be equal to the atomic number for all values of $(\sin\theta)/\lambda$ an at all temperatures. The electron density for a crystal composed of point atoms would show a much higher degree of resolution compared to real crystal.

Figure 2.8 show a plot of the mean value of $|\boldsymbol{F}_0|^2$ against $(\sin\theta)/\lambda$ for typical set of data. The radial decrease in $\overline{|\boldsymbol{F}_0|^2}$ can be reduced by modifying $|\boldsymbol{F}_0|^2$ by a function which increase as $(\sin\theta)/\lambda$ increase. The coefficients for sharpened Patterson synthesis may be calculated by the following equation,

$$|\boldsymbol{F}_{mod}(hkl)|^2 = \frac{|\boldsymbol{F}_0(hkl)|^2}{\exp[-2B(\sin^2\theta)/\lambda]\{\sum_{j=1}^{N} f_j\}^2} \tag{2.55}$$

N is the number of atoms in the unit cell and B is an overall isotropic temperature factor. $|\boldsymbol{F}_{mod}(hkl)|^2$ is used instead of $|\boldsymbol{F}_0|^2$ for the sharpened Patterson function.

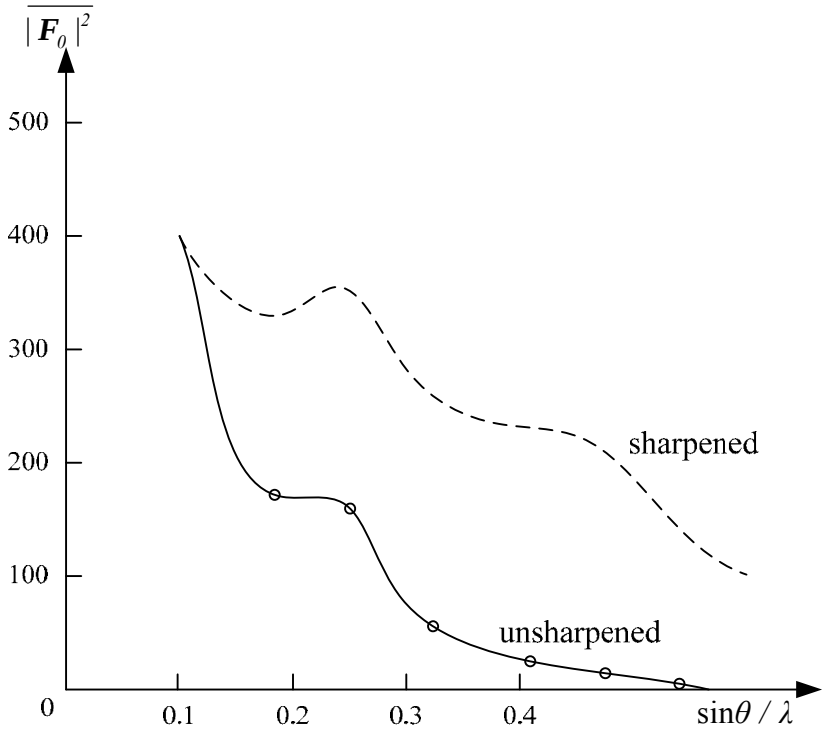

Figure 2.8 – Effects of sharpening on the radial decrease of the local average intensity $|\boldsymbol{F}_0|^2$ (Ladd and Palmer, 1993).

2.9.6 Location of heavy-atom, Harker Plane, Harker Lines and Patterson Superposition

If heavy-atom exists in the crystal, it will dominate the scattering of the structure factor. Heavy atoms can usually be located by analysis of a Patterson map but it is still being influenced by how many heavy–atoms are present and how heavy the atom relative to another atoms.

In order to determine the location of heavy-atom in Patterson map, we have to know the space group of the crystal and also the elements in the crystal. From the elements of the crystal, expected approximate relative heights of typical peaks in Patterson map can be calculated which will be dominated by *"heavy-atom - heavy-atom"* vectors. From the space group, Harker peaks – the interatomic vectors relating the symmetry equivalent atom can be obtained. It will be seen that some of the peaks